Scattering of sound from axisymetric sources by multiple circular cylinders

Scott E. Sherer[a)]
Air Vehicles Directorate, Air Force Research Laboratory, Wright-Patterson AFB, Ohio 45433-7521

(Received 10 January 2003; revised 15 November 2003; accepted 24 November 2003)

A general analytic method for calculating the scattering of sound by multiple rigid circular cylinders arranged in an arbitrary parallel configuration is presented. The sound scattered by this collection of cylinders is generated by a time-periodic, spatially distributed, axisymmetric source located within the domain of interest. A Hankel transform method is used to calculate the incident field, while separation of variables is used to obtain the scattered fields from each cylinder in the collection. The unknown scattering coefficients are determined through the use of general addition theorems that allows the various fields to be readily transformed between coordinate systems. The method is validated using various two-, three-, and four-cylinder configurations, and the number of coefficients that must be retained in the truncated series is examined. Benchmark configurations consisting of two- and three-cylinder systems with cylinders of varying radii are also presented. These solutions have been used to validate computational aeroacoustic solvers developed for complex geometries. [DOI: 10.1121/1.1641790]

PACS numbers: 43.20.Fn [GCG] Pages: 488–496

I. INTRODUCTION

The scattering of waves by two-dimensional circular cylinders is a fundamental problem in both acoustics and electromagnetics. Analytical solutions to the scattering of plane waves by a single circular cylinder are presented by, among others, Morse and Ingard[1] within the context of acoustics and Balanis[2] in electromagnetics. Single-cylinder solutions have also been developed for incident fields other than plane waves. For example, Shenderov[3] presents a solution for the scattering of sound generated by a cylindrical line source from a single, rigid circular cylinder, while Balanis[2] presents the solution for the equivalent electromagnetic problem. Various authors have also developed solutions for single-cylinder scattering with spatially distributed acoustic sources. These include Kurbatskii,[4] who used a Green's function approach to calculate the scattering from a single, rigid, circular cylinder using a source with a Gaussian spatial distribution, and Morris,[5] who developed via a Hankel transform approach solutions for scattering by a single, acoustically permeable, circular cylinder for various spatially distributed sources including Gaussian and circular disk distributions.

Exact and approximate solutions have also been developed for the scattering of plane waves by multiple parallel circular cylinders. One of the earliest solutions to this problem for rigid cylinders was developed by Twersky,[6] who decomposed the total field into an incident field plus higher order scattered field contributions whose coefficients were determined in an iterative manner. Additional solution techniques were later developed by Young and Bertrand[7] as well as Peterson and Ström.[8] In the former, acoustic scattering calculations for a plane wave incident upon two identical, rigid, circular cylinders were performed using both direct matrix inversion and iterative procedures and compared to experimental data. The latter technique used a recursive approach based on the ''T-matrix method''[9] to formulate the scattering from an arbitrary number of general scatterers with a general, nonsingular incident field, although results are only presented for plane-wave scattering from two spheres. A general classification system for the various techniques available to solve the multiple-scattering problem as well as additional references for the multiple-cylinder case is given by Elsherbeni.[10]

Multiple-scattering phenomena have also received considerable attention as related to phononic crystals and wave localization.[11] Within this application, solution methods have been developed by Kafesaki and Economou,[12] which was used by Kafesaki *et al.*[13] to examine the phononic properties of air bubbles in water, and by Psarobas *et al.*,[14] which was employed by Yang *et al.*[15] in their investigation of the phononic properties of tungsten carbide beads in water. Similarly, exact solutions for the localization lengths associated with a random array of air cylinders in a water medium are presented by Gupta and Ye.[16]

In the current work, an analytic method is developed to obtain solutions to the problem of the scattering of sound generated by two types of axisymmetric sources by multiple rigid, circular cylinders of varying radii. The long axes of the cylinders are assumed to be parallel to each other, and thus the problem is two-dimensional. However, the distribution of the cylinders within this two-dimensional plane is arbitrary under the constraint that they do not overlap nor are they in contact with each other. This approach, which is an extension of the single-cylinder work of Morris,[5] utilizes a Hankel transform method to determine the incident field from a spatially distributed acoustic source. Separation of variables provides the general solution for the scattered field from each cylinder in its own coordinate system, and cylindrical addition theorems are employed to allow the application of the

a)Electronic mail: Scott.Sherer@wpafb.af.mil

boundary conditions in the various coordinate systems. The scattering coefficients for all cylinders are solved simultaneously by direct inversion, and thus the approach would be considered a boundary value solution method per the classification scheme of Ref. 10.

The solutions presented here are analytic in nature, although the necessary truncation of infinite series, numerical inversion of potentially ill-conditioned matrices, and the numerical evaluation of certain integrals can result in the generation of numerical error if not addressed. Because it is analytic, this approach is useful for establishing benchmark scattering solutions that may be used to assess the accuracy of computational aeroacoustic solvers developed for geometrically complex configurations.[17–19] The use of solutions generated by a spatially distributed source is preferred over a line source or plane-wave solution for this purpose due to the presence of a singularity in the total field for the former and the requirement to propagate the incident wave into the domain of interest from beyond its boundaries when using the total field formulation for the latter. This analytic approach may also prove amenable to parametric studies of the scattering behavior of systems involving multiple-cylinder geometries.

The following section addresses theoretical analysis, including the formulation of the problem under consideration, its analytic solution, and the acoustic source types considered. The next section contains results obtained for various configurations and source frequencies, including validation studies and investigations of some of the numerical issues associated with this procedure. This section concludes with scattered and total field results obtained for two- and three-cylinder benchmark configurations.

II. THEORETICAL ANALYSIS

A. Problem formulation

The problem considered here is the scattering of sound generated from a time-periodic, axisymmetric source by a set of M parallel, infinitely long (i.e., two-dimensional), rigid, circular cylinders. The arrangement of the cylinders and the source within the unbounded, two-dimensional domain of interest is arbitrary, with the caveat that the cylinders may not be in contact with nor overlap one another. This domain initially consists of a fluid with a speed of sound given by c_∞. A reference length l_{ref}, given by the diameter of the largest cylinder in the collection, and a reference time t_{ref}, given by $t_{\text{ref}}=l_{\text{ref}}/c_\infty$, have been used throughout this work for nondimensionalization purposes. It is also assumed that there is no mean flow in the domain.

The geometric relationships between any two cylinders i and j in this collection, the acoustic source centered at S, and an arbitrary observation point at O are given in Fig. 1. A polar coordinate system (r_i,θ_i) is defined based on the center of cylinder i, while a second polar coordinate system (r_j,θ_j) is defined based on the center of cylinder j. A third polar coordinate system (R,ϕ) is centered on the source. The positions of the cylinders with respect to the source are given in this source-based polar coordinate system as (L_i,α_i) and (L_j,α_j), respectively. The position of the cylinder j in the coordinate system of cylinder i is given by (D_{ij},ψ_{ij}), and likewise the position of the cylinder i in the coordinate system of cylinder j is given by (D_{ji},ψ_{ji}). It is noted that $D_{ij}=D_{ji}$ and $|\psi_{ij}-\psi_{ji}|=\pi$. The radii of the cylinders are denoted by a_i and a_j, respectively, and in general are not equal.

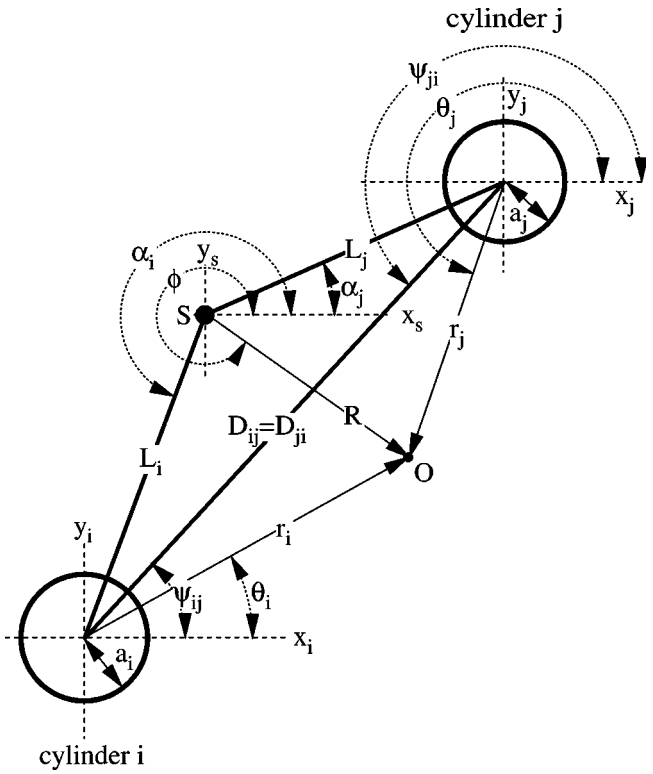

FIG. 1. Schematic showing coordinate system definitions and geometric relationships between acoustic source located at point S, an observation point at point O, and two arbitrary cylinders labeled i and j.

Assuming linear scattering and a time-dependent, axisymmetric source of the form $S(R,t)=f(R)e^{-\iota\omega t}$, the incident field satisfies the nonhomogeneous Helmholtz equation, here written in terms of the source coordinate system as

$$\frac{d^2\Phi^{\text{inc}}}{dR^2}+\frac{1}{R}\frac{d\Phi^{\text{inc}}}{dR}+k^2\Phi^{\text{inc}}=\tilde{f}(R), \tag{1}$$

where $\tilde{f}(R)=-\iota kf(R)$ and $k=\omega/c_\infty$. Note that the ϕ dependence has been dropped due to axisymmetry of the source. Similarly, the scattered field generated by each cylinder independently satisfies the homogeneous Helmholtz equation, written in the local, cylinder-based coordinate system as

$$\frac{\partial^2\Phi_i^s}{\partial r_i^2}+\frac{1}{r_i}\frac{\partial\Phi_i^s}{\partial r_i}+\frac{1}{r_i^2}\frac{\partial^2\Phi_i^s}{\partial\theta_i^2}+k^2\Phi_i^s=0,\quad i=1,2,...,M. \tag{2}$$

The principle of superposition is used to write the total field as the sum of the incident and scattered fields

$$\Phi=\Phi^{\text{inc}}+\sum_{i=1}^{M}\Phi_i^s. \tag{3}$$

The standard rigid-body boundary conditions applied at the surface of each cylinder j thus may be expressed in terms of these fields as

$$\sum_{i=1}^{M} \left.\frac{\partial \Phi_i^s}{\partial r_j}\right|_{r_j=a_j} = -\left.\frac{\partial \Phi^{\text{inc}}}{\partial r_j}\right|_{r_j=a_j} \qquad j=1,2,...,M. \tag{4}$$

B. Solution development

Morris[5] solved Eq. (1) using a Hankel transform method to determine the incident field, given in terms of the source-based coordinate system as

$$\Phi^{\text{inc}}(R) = -\int_0^\infty \frac{sJ_0(sR)\tilde{F}(s)}{(s^2-k^2)}ds, \tag{5}$$

where $\tilde{F}(s)$ is the Hankel transform of the spatial source distribution $\tilde{f}(R)$

$$\tilde{F}(s) = \int_0^\infty RJ_0(sR)\tilde{f}(R)dR, \tag{6}$$

and J_n is the Bessel function of the first kind of order n. Likewise, the solution for each scattered field may be obtained by solving Eq. (2) using separation of variables. Invoking an outgoing radiation boundary condition at infinity for the $e^{-\imath\omega t}$ time dependency, the scattered field from the ith cylinder is written in its local coordinate system as

$$\Phi_i^s(r_i,\theta_i) = A_{0i}H_0(kr_i) + \sum_{n=1}^{\infty} H_n(kr_i)[A_{ni}\cos(n\theta_i) + B_{ni}\sin(n\theta_i)] \tag{7}$$

where H_n is the Hankel function of the first kind of order n.

The scattered field coefficients A_{ni} and B_{ni} from Eq. (7) are found though the application of the M boundary conditions given by Eq. (4). This is accomplished through the application of the Graf addition theorem,[20] which allows the incident and scattered fields to be written in terms of the coordinate system of each cylinder in order to apply the boundary conditions at its surface. Using this theorem, the Bessel and Hankel functions in Eqs. (5) and (7) are written in terms of the coordinate system of cylinder j as

$$J_0(kR) = \sum_{m=0}^{\infty} \epsilon_m(-1)^m J_m(kL_j)J_m(kr_j) \times[\cos(m\alpha_j)\cos(m\theta_j) + \sin(m\alpha_j)\sin(m\theta_j)], \tag{8}$$

and

$$H_n(kr_i)\cos(n\theta_i) = \sum_{m=0}^{\infty} \frac{\epsilon_m}{2}\{[(-1)^m\mathcal{K}_{ijmn}^{c+} + \mathcal{K}_{ijmn}^{c-}]\cos(m\theta_j) + [(-1)^m\mathcal{K}_{ijmn}^{s+} - \mathcal{K}_{ijmn}^{s-}]\sin(m\theta_j)\}, \tag{9}$$

$$H_n(kr_i)\sin(n\theta_i) = \sum_{m=0}^{\infty} \frac{\epsilon_m}{2}\{[(-1)^m\mathcal{K}_{ijmn}^{s+} + \mathcal{K}_{ijmn}^{s-}]\cos(m\theta_j) - [(-1)^m\mathcal{K}_{ijmn}^{c+} - \mathcal{K}_{ijmn}^{c-}]\sin(m\theta_j)\}, \tag{10}$$

where ϵ_m is the Neumann factor, defined as

$$\epsilon_m = \begin{cases} 1 & m=0 \\ 2 & m\geqslant 1 \end{cases}, \tag{11}$$

and

$$\mathcal{K}_{ijmn}^{(c,s)\pm} = H_{n\pm m}(kD_{ij})J_m(kr_j)\cdot\begin{cases}\cos[(n\pm m)\psi_{ij}] \\ \sin[(n\pm m)\psi_{ij}]\end{cases}. \tag{12}$$

It is noted that the transformations for the Hankel functions are only valid for $r_j<D_{ij}$, but that this condition will always be satisfied on the surface of the cylinders where the boundary conditions are evaluated provided they are neither overlapping nor in contact with one another.

Using the previous transformations in conjunction with the incident and scattered fields given by Eqs. (5) and (7), the coefficients A_{ni} and B_{ni} may be determined through the application of the boundary conditions as given by Eq. (4) on the surface of each cylinder. The resulting M equations consist of infinite summations on both the left- and right-hand side of the equality, with each term possessing a factor of $\cos(m\theta_j)$, or of $\sin(m\theta_j)$, or having no θ_j dependency at all (the $m=0$ case). Equating on a term-by-term basis and truncating the infinite series at some finite value N yields $(2N+1)$ equations for each cylinder, or $M\cdot(2N+1)$ equations for the entire cylinder set. These equations are linear with respect to the $M\cdot(2N+1)$ unknown coefficients A_{ni} and B_{ni}, and may be expressed concisely in matrix form as

$$Z\mathbf{x} = \mathbf{b}. \tag{13}$$

The matrix Z may be written in terms of M^2 submatrices of dimension $(2N+1)\times(2N+1)$ as

$$Z = \begin{bmatrix} \mathcal{Z}_{11} & \mathcal{Z}_{12} & \cdots & \mathcal{Z}_{1M} \\ \mathcal{Z}_{21} & \mathcal{Z}_{22} & \cdots & \mathcal{Z}_{2M} \\ \vdots & \vdots & \ddots & \vdots \\ \mathcal{Z}_{M1} & \mathcal{Z}_{M2} & \cdots & \mathcal{Z}_{MM} \end{bmatrix}. \tag{14}$$

The off-diagonal submatrices $\mathcal{Z}_{ij}$, $i\neq j$, may be further subdivided as

$$\mathcal{Z}_{ij} = \begin{bmatrix} \mathcal{C}_{ij}^{+} & \mathcal{S}_{ij}^{+} \\ \mathcal{S}_{ij}^{-} & -\mathcal{C}_{ij}^{-} \end{bmatrix}, \tag{15}$$

where the elements of these submatrices are given by

$$[(\mathcal{C},\mathcal{S})_{ij}^{\pm}]_{mn} = \frac{\epsilon_m}{2}\overline{\mathcal{K}}_{jimn}^{(c,s)\pm} \rightarrow \begin{cases} \mathcal{C}^+:\{m=0\rightarrow N, n=0\rightarrow N\} \\ \mathcal{S}^+:\{m=0\rightarrow N, n=1\rightarrow N\} \\ \mathcal{S}^-:\{m=1\rightarrow N, n=0\rightarrow N\}, \\ \mathcal{C}^-:\{m=1\rightarrow N, n=1\rightarrow N\} \end{cases} \tag{16}$$

with

$$\overline{\mathcal{K}}_{ijmn}^{(c,s)\pm} = (-1)^m\mathcal{K}_{ijmn}^{(c,s)+\prime} \pm \mathcal{K}_{ijmn}^{(c,s)-\prime}, \tag{17}$$

and from Eq. (12)

$$\mathcal{K}_{ijmn}^{(c,s)\pm\prime}=\left.\frac{\partial \mathcal{K}_{ijmn}^{(c,s)\pm}}{\partial r_j}\right|_{r_j=a_j}$$
$$=\frac{k}{2}H_{m\pm n}(kD_{ij})[J_{m-1}(ka_j)-J_{m+1}(ka_j)]$$
$$\cdot\begin{Bmatrix}\cos[(n\pm m)\psi_{ij}]\\ \sin[(n\pm m)\psi_{ij}]\end{Bmatrix}. \tag{18}$$

The submatrices $\mathcal{Z}_{jj}$ on the diagonal of Eq. (14) are themselves diagonal matrices of the form

$$\mathcal{Z}_{jj}=\begin{bmatrix} H'_{0j} & & & & & & \\ & \ddots & & & & 0 & \\ & & H'_{Nj} & & & & \\ & & & H'_{1j} & & & \\ & 0 & & & \ddots & & \\ & & & & & H'_{Nj} \end{bmatrix}, \tag{19}$$

where

$$H'_{nj}=\left.\frac{\partial H_n(kr_j)}{\partial r_j}\right|_{r_j=a_j}=\frac{k}{2}[H_{n-1}(ka_j)-H_{n+1}(ka_j)]. \tag{20}$$

The solution and right-hand-side vectors may also be expressed in block form as

$$\mathbf{x}=\begin{bmatrix}\boldsymbol{\mathcal{X}}_1\\ \boldsymbol{\mathcal{X}}_2\\ \vdots\\ \boldsymbol{\mathcal{X}}_M\end{bmatrix}\rightarrow\boldsymbol{\mathcal{X}}_i=\begin{bmatrix}A_{0i}\\ A_{1i}\\ \vdots\\ A_{Ni}\\ B_{1i}\\ B_{2i}\\ \vdots\\ B_{Ni}\end{bmatrix}, \tag{21}$$

and

$$\mathbf{b}=\begin{bmatrix}\boldsymbol{\mathcal{B}}_1\\ \boldsymbol{\mathcal{B}}_2\\ \vdots\\ \boldsymbol{\mathcal{B}}_M\end{bmatrix}\rightarrow\boldsymbol{\mathcal{B}}_j=\begin{bmatrix}I_{0j}^{c\prime}\\ I_{1j}^{c\prime}\\ \vdots\\ I_{Nj}^{c\prime}\\ I_{1j}^{s\prime}\\ I_{2j}^{s\prime}\\ \vdots\\ I_{Nj}^{s\prime}\end{bmatrix}, \tag{22}$$

with

$$I_{mj}^{(c,s)\prime}=\frac{\epsilon_m}{2}(-1)^m\int_0^\infty\frac{s^2J_m(sL_j)[J_{m-1}(sa_j)-J_{m+1}(sa_j)]\tilde{F}(s)}{s^2-k^2}ds\cdot\begin{Bmatrix}\cos(m\alpha_j)\\ \sin(m\alpha_j)\end{Bmatrix} \tag{23}$$

Upon solving this system of equations for the coefficients A_{ni} and B_{ni}, the scattered and total fields may be found via Eqs. (7) and (3), respectively.

C. Acoustic source types

To determine the incident field given by Eq. (5) and the right-hand-side vector **b** using the definitions in Eqs. (22) and (23), a specific form of $\tilde{F}(s)$ is required. Two particular source types will be considered here: a cylindrical line source and a spatially distributed cylindrical source with a Gaussian spatial distribution. Morris[5] previously considered both of these source types for the single-cylinder case, and the reader is referred there for more detail.

For the cylindrical line source, the spatial source function $f(R)$ and its corresponding Hankel-transformed counterpart $\tilde{F}(s)$ are given by

$$f(R)=\frac{\delta R}{2\pi R}\rightarrow\tilde{F}(s)=\frac{-\iota k}{2\pi}, \tag{24}$$

where $\delta(R)$ is the Dirac delta function. Integrating in the complex plane and applying the residue theorem yields for the incident field

$$\Phi^{\text{inc}}(R)=-\frac{k}{4}H_0(kR). \tag{25}$$

Likewise, the components making up the vector **b** are given by

$$I_{mj}^{(c,s)\prime}=\frac{\epsilon_m k^2}{8}(-1)^mH_m(kL_j)[J_{m-1}(ka_j)$$
$$-J_{m+1}(ka_j)]\cdot\begin{Bmatrix}\cos(m\alpha_j)\\ \sin(m\alpha_j)\end{Bmatrix}. \tag{26}$$

The second source type considered here is a spatially distributed source of the form

$$f(R)=\exp(-dR^2)\rightarrow\tilde{F}(s)=\frac{-\iota k}{2d}\exp\left(-\frac{s^2}{4d}\right). \tag{27}$$

For this source, the integrals in Eqs. (5) and (23) cannot be integrated analytically. The approach used by Morris[5] to perform the integration numerically is instead used with some minor modifications. In this approach, the variable of integration s is replaced by a new variable τ such that

$$s=\tau-\iota\gamma\exp[-\beta(\tau-k)^2], \tag{28}$$

where $\gamma=k/10$ and $\beta=-\ln(1\times10^{-10}/\gamma)/k^2$. The curve defined by the new variable τ is deformed below the real axis,

thus by-passing the pole located at $s=k$ and allowing the numerical integration to proceed. While in Ref. 5 a ten-point Gauss–Legendre integration scheme was employed over individual intervals of length $k/40$ along the integration path, here the numerical integration is performed by the software package MATHEMATICA.[21] This approach allows for intervals of various lengths to be employed while still maintaining a specified error tolerance. The use of larger intervals in those regions that can be numerically integrated by MATHEMATICA to the specified precision decreases the time it takes to calculate the value of the integral over the entire path. Even so, with $M\cdot(N+1)$ integrals required to construct the right-hand side of Eq. (13), the numerical integration of Eq. (23) is still the most time-consuming aspect of calculating the scattering coefficients. Note that the selection of this contour is not unique, and that other contours may be used to perform the numerical integration.

III. RESULTS AND DISCUSSION

All results presented in this work are normalized by the value of the incident field at a distance $R=L_1$ from the source, i.e., the distance from the source to the center of the left-most cylinder in a given configuration.

A. Implementation and validation

To obtain the incident and scattered fields for the various situations examined here, the previously presented formulation was coded in MATHEMATICA. This software package was used to solve the linear system of equations given by Eq. (13) and to perform the necessary numerical integrations for the cases involving the spatially Gaussian source. As discussed in the Introduction, there are several issues associated with the numerical implementation of this approach. These include the truncation of the infinite summations in the series solution for the scattered fields and in application of the addition theorems, the potential for the coefficient system to be ill-conditioned, and the numerical evaluation of the integrals required for the spatially Gaussian source. These issues will now be discussed.

The issue of ill-conditioning arises from the potential disparity in the eigenvalues of the coefficient matrix $\mathcal{Z}$ as additional terms are retained in the series solution for the scattered fields. Two methods were employed to address this issue. First, only the minimum number of scattering coefficients required to obtain a converged solution was retained, as the condition number of the coefficient matrix grows rapidly as additional terms are included. Second, partial pivoting was used in conjunction with Gaussian elimination to find the scattered coefficients, which helps to limit any round-off error.[22] To test the effectiveness of these steps, several of the cases shown in this work were solved using various levels of precision by first calculating the elements of the coefficient matrix and right-hand-side vector using exact algebra, and then evaluating them to a specified precision before solving the linear system. For all cases examined, the precision of the solutions obtained was comparable to the original precision used to generate the matrix elements, i.e., solutions generated using four digits of precision matched solutions obtained with higher precision to the first four decimal places. Thus, the lack of accuracy in the coefficient matrix and right-hand-side vectors did not result in large changes in the solution, indicating that the steps taken to address potential ill-conditioning of the matrix were effective.

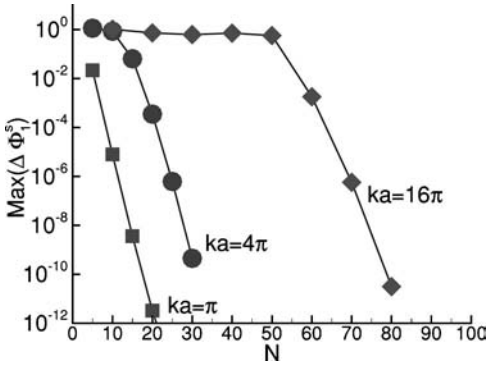

FIG. 2. Numerical convergence behavior for two-cylinder configuration with various values of ka. $\Delta\Phi_1^s$ represents the maximum change for the surface scattered field between solutions generated with N and $N+\Delta N$ terms.

Next, the issue of number of terms needed to obtain a converged solution is examined. For plane-wave scattering from symmetric, two-cylinder configurations, Young and Bertrand[7] and Decanini *et al.*[23] give empirical expressions for the value of N as

$$N=2ka+Q, \quad Q=\begin{cases}5-10, & ka\leqslant 1\\ 0, & ka>1,\end{cases} \tag{29}$$

and

$$N=\max\{8,[ka+4(ka)^{1/3}+1]\}, \tag{30}$$

respectively. Here, the number of terms required for a given level of accuracy is evaluated for two particular configurations. The first consists of three identical cylinders located at the vertices of an equilateral triangle with sides of length 3 and a line source located at the centroid of the configuration. The second consists of two identical cylinders separated by a distance of 8, with a spatially Gaussian source given by Eq. (27), where $d=25\ln 2$ located midway between them. To check convergence, the scattered field at the surface of one of the cylinders was tracked as the value of N was increased by steps of ΔN. The maximum difference between the scattered field obtained with N coefficients and the scattered field obtained with $N+\Delta N$ is plotted in Fig. 2 for the two-cylinder configuration and Fig. 3 for the three-cylinder configuration for various values of ka. Here, $\Delta N=5$ for all cases except the $ka=16\pi$ case, in which $\Delta N=10$. Examination of these figures shows that the formula given by Eq. (30) matches very well with the number of terms required to obtain a converged solution, here defined as truncation errors of less than 10^{-6}. However, the simpler formula given by Eq. (29) underpredicts the number of coefficients required at the lowest value of $ka=\pi$ and overpredicts N at the highest value of $ka=16\pi$. Thus, Eq. (30) was used to determine an initial value of N to use for subsequent calculations, although slightly higher values of N were also used to verify convergence.

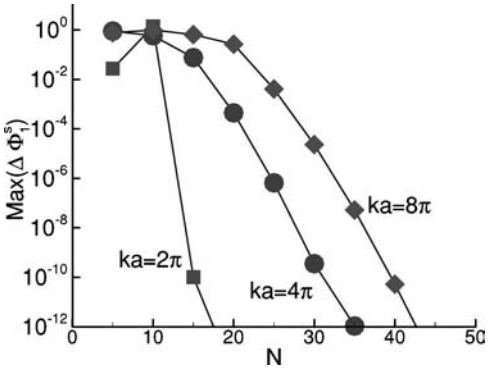

FIG. 3. Numerical convergence behavior for three-cylinder configuration with various values of ka. $\Delta\Phi_1^s$ represents the maximum change for the surface scattered field between solutions generated with N and $N+\Delta N$ terms.

Various validation checks were performed on the multi-scattering formulation presented here in order to verify its consistency. For the single-cylinder scattering case, the scattering coefficients from this formulation were found to degenerate to those presented by Morris[5] in the rigid-body limit. It was also verified that the formulation yielded the same results for configurations that were different numerically but nearly identical acoustically, i.e., configurations that have a different number of cylinders but, because of the size and/or locations of one or more of the cylinders, appear from an acoustic standpoint to be the same. Results from two such cases are shown in Fig. 4. In the first case, computed with $k=8\pi$, an initially symmetric two-cylinder configuration is degenerated into a one-cylinder configuration by fixing the location and size of one of the cylinders and either incrementally increasing the distance between the source and the other cylinder towards infinity or incrementally decreasing its radius towards zero. The second case, with $k=2\pi$, involved the degeneration of an initially symmetric four-cylinder configuration into a symmetric two-cylinder configuration by fixing the two cylinders on opposite sides of the source and either increasing the distances between the source and the other two cylinders in opposite directions, or decreasing the radii of these two cylinders. Figure 4 plots the scattered field in the backscatter direction (along the line connecting the source and cylinder centers) on the surface of a fixed cylinder versus the parameter n, which controls either the distance between the cylinders being acoustically removed and the source via the formula $L=2^n$, or radii of the removed cylinders via $a=(\frac{1}{2})^n$. For all cases, the results obtained by acoustically removing one or more cylinders from consideration match those obtained if the removed cylinders were never considered. Additional validation was also provided by comparison with numerical results obtained for various two- and three-cylinder configurations via a finite-difference time-domain computational aeroacoustics code.[17,18]

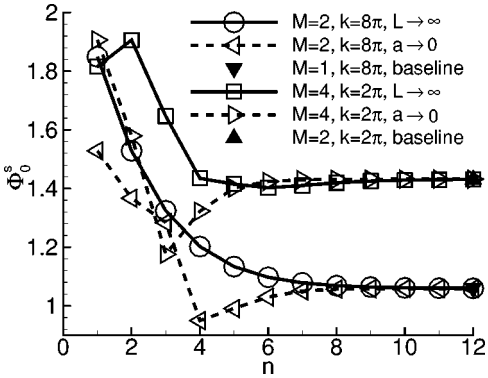

FIG. 4. Scattered field behavior in the backscatter direction for two- and four-cylinder configurations as cylinder(s) are acoustically removed from problem either by increasing the distance between the cylinder(s) and the source ($L\to\infty$) or decreasing their radii ($a\to 0$).

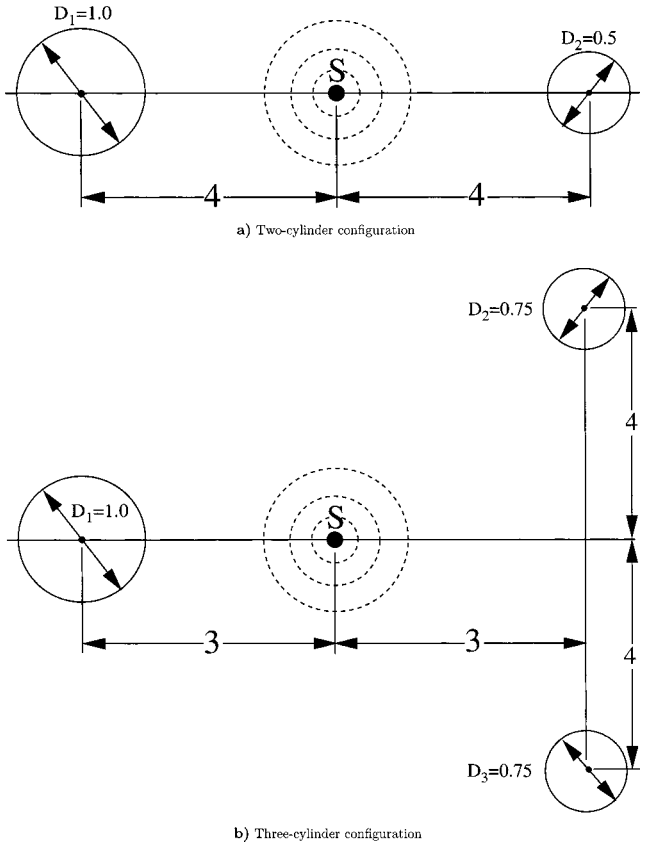

FIG. 5. Benchmark acoustic scattering geometries. (a) Two-cylinder configuration. (b) Three-cylinder configuration.

B. Two- and three-cylinder benchmark configurations

Two specific cases are considered here to provide benchmark results for use in the validation of computational aeroacoustic methods developed for complex geometries.[19] These consist of a two-cylinder configuration and a three-cylinder configuration as shown in Fig. 5. Both cases are symmetric about the centerline axis (the axis connecting the centers of the left-most cylinder and the source), but are asymmetric about the perpendicular axis. Each case was solved with $k=8\pi$ using both line and spatially distributed Gaussian sources, where $d=25\ln 2$ for the latter. Results presented here include the scattered and total root-mean-squared (rms) fields on the surface of the cylinders and the total rms fields along the centerline. These are shown in Figs. 6 through 9 for the two-cylinder configuration, and in Figs. 10 through 13 for the three-cylinder configuration. It is observed that the

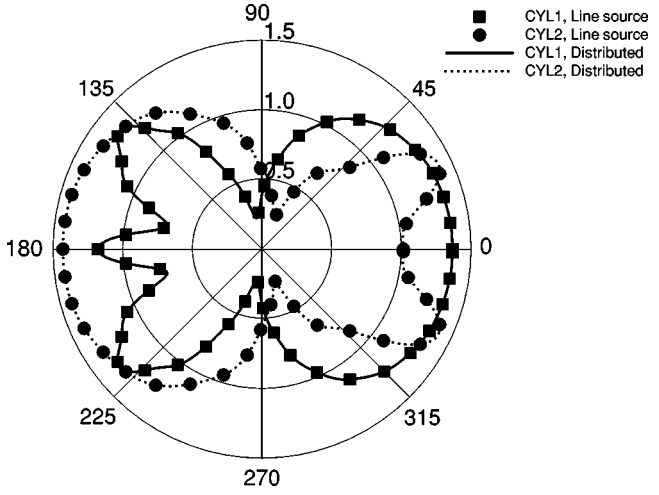

FIG. 6. Scattered field on surfaces of the cylinders for the two-cylinder configuration shown in Fig. 5(a).

line source and spatially distributed Gaussian source produce nearly identical results everywhere except in the immediate vicinity of the source. In this region, the total fields generated by the spatially distributed source begin increasing further away from the source center compared to the field generated by the point source. However, the total field associated with the distributed source remains finite everywhere, while the total field for the line source becomes infinite at the source center.

For the two-cylinder configuration, the scattered field and total rms field on the surface of each cylinder are shown in Figs. 6 and 7, respectively. They are characterized by a smooth variation on the insonified faces of the cylinders. The fields on the quiet sides of the cylinders exhibit more variation, although the magnitude of the total field in Fig. 7 is considerably less on the quiet faces compared to the insonified faces due to the higher incident field magnitudes there. Due to its larger radius, the cylinder to the left of the source exhibits more variation, both in terms of the number of peaks and nulls in the field strength as well as the range between them, over its quiet face compared to the smaller, right-hand cylinder. However, the peak total field on the surface at the point directly facing the source is slightly higher for the smaller cylinder due to the greater scattered field it is exposed to from the larger cylinder. The total rms field calculated along the centerline is shown in Figs. 8 and 9. In both figures, the field along the centerline between the source and the cylinders is highly oscillatory, with a smooth variation in peak and null magnitudes. The behavior of the total field in the shadowed regions is characterized by a slight rise in magnitude near the cylinders followed by a gradual decline as the distance from the cylinder is increased.

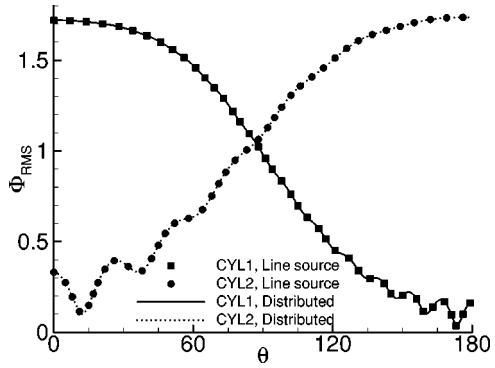

FIG. 7. Total rms field on surfaces of the cylinders for the two-cylinder configuration shown in Fig. 5(a).

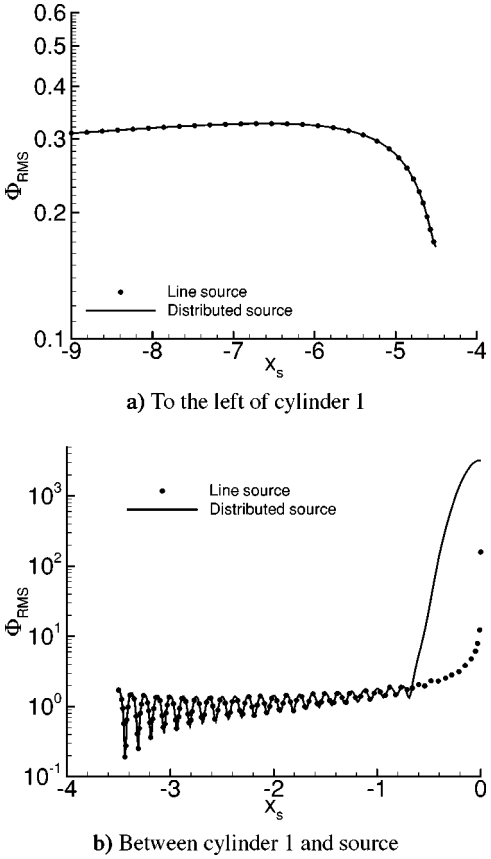

FIG. 8. Total rms field on the centerline to the left of the source for the two-cylinder configuration shown in Fig. 5(a). (a) To the left of cylinder 1. (b) Between cylinder 1 and source.

The scattered and total rms fields on the surfaces of the left- and top-right cylinders in the three-cylinder configuration are shown in Figs. 10 and 11. The surface fields for the three-cylinder case show considerably more variation with angular position than was seen in the two-cylinder case, both on the insonified faces (between approximately 143 and 323 degrees for the top-right cylinder) and on the quiet faces. Because the cylinders to the right of the source experience the incoming incident and scattered fields from different directions, no angular symmetry exists for these two cylinders. The centerline mean-squared total field is shown in Figs. 12 and 13 and also exhibits more complexity than was seen in the two-cylinder case, as the magnitudes of the peaks and nulls themselves vary in an oscillatory manner between the left cylinder and the source. Also, the field in the shadow region, while still diminishing at larger distances from the cylinder, shows additional variation due to the more complex scattering geometry that was not seen in the two-cylinder case.

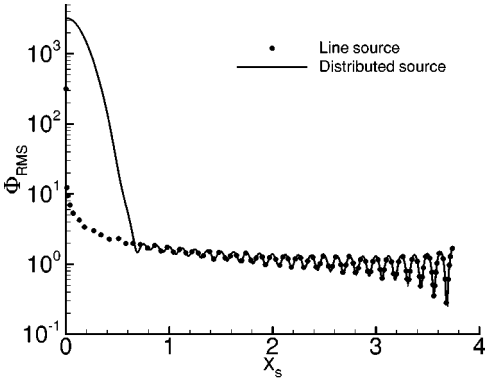

a) Between source and cylinder 2

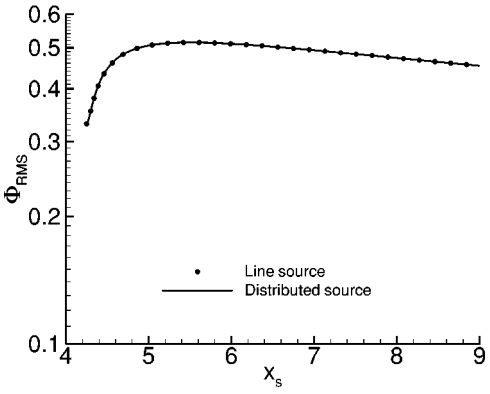

b) To the right of cylinder 2

FIG. 9. Total rms field on the centerline to the right of the source for the two-cylinder configuration shown in Fig. 5(a). (a) Between source and cylinder 2. (b) To the right of cylinder 2.

IV. CONCLUSIONS

An analytic method for evaluating the scattered fields created by a collection of rigid, two-dimensional, circular cylinders when exposed to an incident field generated by two types of axisymmetric sources has been developed. The source types considered here include a cylindrical line source and a source with a Gaussian spatial distribution. The approach uses a Hankel transform method to determine the incident field, and separation of variables to find the scattered fields from each cylinder in the collection. The unknown scattering coefficients are then determined through the solution of a linear system of equations obtained from the simultaneous application of boundary conditions on the surfaces of all cylinders. For a line source, analytic expressions for all terms in this system of equations may be obtained, while numerical evaluation of some integrals is required for the spatially distributed source. Various two-, three-, and four-cylinder symmetric configurations were examined for validation purposes and to investigate the number of coefficients required to obtain a converged solution. Also, results are presented for asymmetric two- and three-cylinder con-

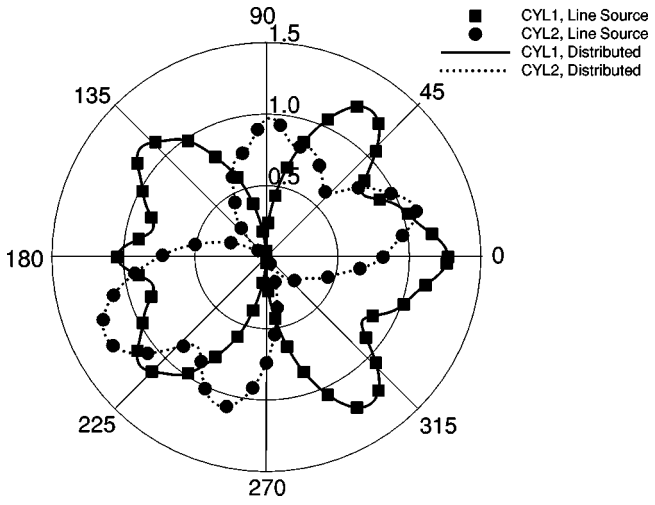

FIG. 10. Scattered field on surfaces of the left and top-right cylinders for the three-cylinder configuration shown in Fig. 5(b).

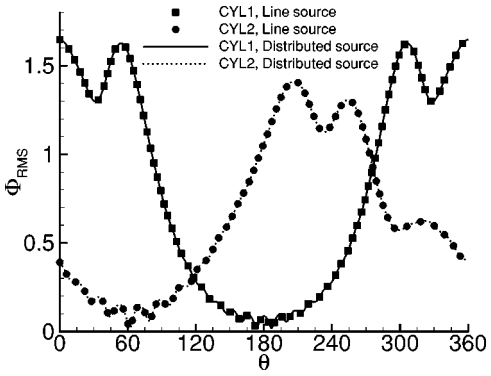

FIG. 11. Total rms field on surfaces of the left- and top-right cylinders for the two-cylinder configuration shown in Fig. 5(b).

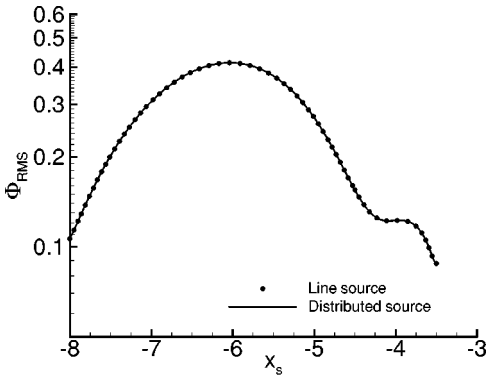

a) To the left of cylinder 1

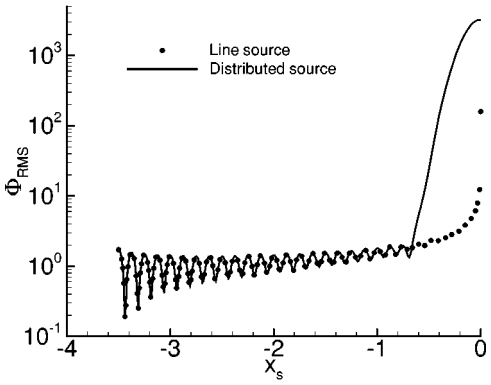

b) Between cylinder 1 and the source

FIG. 12. Total rms field on the centerline to the left of the source for the three-cylinder configuration shown in Fig. 5(b). (a) To the left of cylinder 1. (b) Between cylinder 1 and the source.

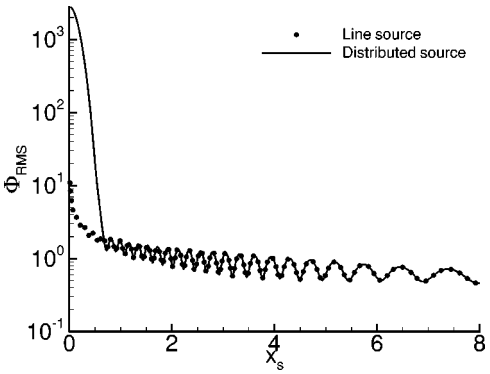

FIG. 13. Total rms field on the centerline to the right of the source for the three-cylinder configuration shown in Fig. 5(b).

figurations that have proved useful for the validation of computational aeroacoustic codes developed for complex geometries.

ACKNOWLEDGMENTS

The author wishes to thank Dr. Phillip Morris for providing FORTRAN versions of his numerical integration routine for examination. The author would also like to thank Dr. Donald Rizzetta and Dr. Miguel Visbal as well as the referees of this work for their reviews of the manuscript and helpful comments provided.

[1] P. Morse and K. Ingard, *Theoretical Acoustics* (McGraw-Hill, New York, 1968).
[2] C. A. Balanis, *Advanced Engineering Electromagnetics*, 1st ed. (Wiley, New York, 1989).
[3] E. Shenderov, ''Diffraction of a cylindrical sound wave by a cylinder,'' Sov. Phys. Acoust. **7**, 293–296 (1962).
[4] K. A. Kurbatskii, ''Analytical Solutions of the Category 1, Benchmark Problems 1 and 2,'' Second Computational Aeroacoustic (CAA) Workshop on Benchmark Problems, NASA CP-3352, 1997, pp. 9–14.
[5] P. J. Morris, ''The scattering of sound from a spatially distributed symmetric cylindrical source by a circular cylinder,'' J. Acoust. Soc. Am. **97**, 2651–2656 (1995).
[6] V. Twersky, ''Multiple scattering of radiation by an arbitrary configuration of parallel cylinders,'' J. Acoust. Soc. Am. **24**, 42–46 (1952).
[7] J. Young and J. Bertrand, ''Multiple scattering by two cylinders,'' J. Acoust. Soc. Am. **58**, 1190–1195 (1975).
[8] B. Peterson and S. Ström, ''Matrix formulation of acoustic scattering from an arbitrary number of scatterers,'' J. Acoust. Soc. Am. **56**, 771–780 (1974).
[9] P. Waterman, ''New formulation of acoustic scattering,'' J. Acoust. Soc. Am. **45**, 1417–1429 (1969).
[10] A. Elsherbeni, ''A comparative study of two-dimensional multiple scattering techniques,'' Radio Sci. **29**, 1023–1033 (1994).
[11] J. Vasseur, P. Deymier, B. Chenni, B. Djafari-Rouhani, L. Dobrzynski, and D. Prevost, ''Experimental and theoretical evidence for the existence of absolute acoustic band gaps in two-dimensional solid phononic crystals,'' Phys. Rev. Lett. **86**, 3012–3015 (2001).
[12] M. Kafesaki and E. Economou, ''Multiple-scattering theory for three-dimensional periodic acoustic composites,'' Phys. Rev. B **60**, 11993–12001 (1999).
[13] M. Kafesaki, R. Penciu, and E. Economou, ''Air bubbles in water: A strongly multiple scattering medium for acoustic waves,'' Phys. Rev. Lett. **84**, 6050–6053 (2000).
[14] I. Psarobas, N. Stefanou, and A. Modinos, ''Scattering of elastic waves by periodic arrays of spherical bodies,'' Phys. Rev. B **62**, 278–291 (2000).
[15] S. Yang, J. Page, Z. Liu, M. Cowan, C. Chan, and P. Sheng, ''Ultrasound tunneling through 3D phononic crystals,'' Phys. Rev. Lett. **88**, 104301 (2002).
[16] B. Gupta and Z. Ye, ''Localization of classical waves in two-dimensional random media: A comparison between the analytic theory and exact numerical simulation,'' Phys. Rev. E **67**, 036606 (2003).
[17] S. Sherer and M. Visbal, ''Computational study of acoustic scattering from multiple bodies using a high-order overset grid approach,'' AIAA Paper 2003-3203, 9th AIAA/CEAS Aeroacoustics Conference, Hilton Head, SC, June 2003.
[18] S. E. Sherer, ''Further analysis of high-order overset grid method with applications,'' AIAA Paper 2003-3839, AIAA 16th Computational Fluid Dynamics Conference, Orlando, FL, June 2003.
[19] Fourth Computational Aeroacoustic (CAA) Workshop on Benchmark Problems, NASA Conference Proceeding, 2004.
[20] M. Abramowitz and I. A. Stegun, *Handbook of Mathematical Functions with Formulas, Graphs and Mathematical Tables*, 5th ed. (Dover, New York, 1968).
[21] S. Wolfram, *The Mathematica Book* (Cambridge University Press, New York, 1999).
[22] G. Strang, *Linear Algebra and Its Applications*, 3rd ed. (Harcourt Brace, New York, 1988).
[23] Y. Decanini, A. Folacci, P. Gabrielli, and J.-L. Rossi, ''Algebraic aspects of multiple scattering by two parallel cylinders: Classification and physical interpretation of scattering resonances,'' J. Sound Vib. **221**, 785–804 (1999).